Research Article

Jiqing Han*, Qiuping Feng, and Li Zhang*

Clean preparation of rutile from Ti-containing mixed molten slag by CO_2 oxidation

https://doi.org/10.1515/gps-2023-0083
received May 28, 2023; accepted August 14, 2023

Abstract: The effects of SiO_2 and CO_2 on the crystallization action of Ti-containing mixed molten slag (molten Ti-containing blast furnace slag and molten Ti slag) were discussed by thermodynamic calculation and specific experiments. The results of thermodynamic calculation indicated that the increase of SiO_2 addition mass and CO_2 oxidation time can promote the transformation of anosovite and sphene to rutile. The experiment results showed that the phase composition of modification slag was only rutile under the SiO_2 addition mass of 110 g and the CO_2 oxidation time of 180 s. Moreover, the formation theory of rutile was investigated. Using CO_2 as an oxidizing gas can not only prepare rutile but also achieve carbon neutrality, which is a clean preparation method.

Keywords: Ti-containing blast furnace slag, CO_2 oxidation, rutile, titanium slag

1 Introduction

China has rich Ti resources, which mainly are present as V–Ti magnetite. Its total reserve is approximately 10 billion tons, 90% of which are located in the Panzhihua and Xichang regions of Sichuan province. After beneficiation, 50% of titanium components enter the V–Ti magnetite concentrate. After blast furnace ironmaking, the Ti components in the concentrate enter the slag to form Ti-containing blast furnace slag (20–25% TiO_2). The multipurpose use of Ti-containing blast furnace slag has been a technical difficulty in China. Because the Ti compositions in this slag are dispersedly distributed in different fine Ti-containing phases, conventional beneficiation methods make it difficult to separate the Ti-containing phase from the gangue phase. Therefore, the multipurpose use of Ti-containing blast furnace slag is extremely difficult.

To realize the multipurpose use of Ti-containing blast furnace slag, a lot of related studies have been carried out. According to the classification of products, research methods can be divided into the following categories: building materials [1], titanium alloy [2], photocatalytic materials [3], titanium white [4], titanium tetrachloride [5], perovskite [6], anosovite [7,8], and rutile [9–16]. Although the previous methods can realize the multipurpose use of Ti-containing blast furnace slag, they generally have the disadvantages of high energy consumption and high cost. So far, Ti-containing blast furnace slag can only be stacked in the slag yard, causing the squander of Ti resources and environmental pollution.

To resolve the above-mentioned problems, the platform technology [17] for molten slag metallurgy, mineral regeneration, and resource recycling were proposed by Professor Zhang Li of Northeastern University. In view of the mineral characteristics of metallurgical molten slag, a separation technology for oxide mineral settling was proposed for the first time to realize the efficient utilization of physical heat and the efficient recovery of minerals. The platform technology is developed by the interdisciplinary integration of geology, minerals, materials, metallurgy, and thermal energy. It has the characteristics of short process, low cost, cleanness, low carbon, and high efficiency. It does not require heating or a small amount of heating and realizes energy utilization, mineral regeneration, resources recycling, and environmental protection.

Based on the platform technology, the clean, high-efficiency, and low-carbon utilization technology of Ti-containing mixed molten slag (molten Ti-containing blast furnace slag and molten Ti slag) was proposed. This technology consists of two parts:

1. Mineral regeneration: Taking full the merits of the high physical heat and chemical activity of molten Ti-containing blast furnace slag and molten Ti slag, the two molten slags are mixed. With the help of oxidation and

* **Corresponding author: Jiqing Han,** School of Digital Equipment, Jiangsu Vocational College of Electronics and Information, Huai'an 223003, China, e-mail: hanjiqing007@163.com
* **Corresponding author: Li Zhang,** School of Metallurgy, Northeastern University, Shenyang 110819, China, e-mail: fantai320@163.com
Qiuping Feng: School of Digital Equipment, Jiangsu Vocational College of Electronics and Information, Huai'an 223003, China

modification, Ti components form a man-made mineral (rutile) with a high melting temperature, high density, and high crystallization temperature. The impurity components form a glassy phase with a low melting temperature, low density, and low crystallization temperature.

2. Rutile settling: Under the action of crystallization differentiation and gravity differentiation, the man-made mineral (rutile) begins to settle, realizing the transformation from lean ore into rich ore.

The previous studies [18–20] have achieved the transformation of Ti components in Ti-containing mixed molten slag to rutile by O_2 oxidation. In this article, the preparation of rutile from Ti-containing mixed molten slag by CO_2 oxidation was first proposed. Using CO_2 as an oxidizing gas can not only prepare rutile but also achieve carbon neutrality, which is a clean preparation method.

The objective of this article is to propose a method for the clean preparation of rutile from Ti-bearing mixed molten slag by CO_2 oxidation. The effects of SiO_2 and CO_2 on the crystallization action of the Ti-containing mixed molten slag were studied by thermodynamic calculation and specific experiments. Furthermore, the formation theory of rutile was investigated.

Table 1: Chemical components of (1) Ti-containing blast furnace slag and (2) Ti slag

NO.	TiO_2	Ti_2O_3	CaO	SiO_2	Al_2O_3	MgO	MFe	FeO
1	17.58	3.86	26.87	25.13	14.08	7.86	2.18	1.51
2	60.72	14.65	4.32	8.85	2.64	2.02	0.96	—

Note: %, mass fraction; MFe is the content of metallic iron.

2 Materials and methods

2.1 Materials

Ti-containing blast furnace slag and Ti slag were gotten from the Panzhihua (Sichuan province, China). The chemical components and phase compositions of Ti-containing blast furnace slag and Ti slag are illustrated in Table 1 and Figure 1.

As illustrated in Figure 1, the phase components of Ti-containing blast furnace slag were perovskite, magnesia-alumina spinel, diopside, and akermanite. The phase components of Ti slag were anosovite and anorthite.

2.2 Experimental procedures

2.2.1 Thermodynamic calculation

The schematic diagram of experimental process is shown in Figure 2. As illustrated in Figure 2, the effects of SiO_2 and CO_2 on the crystallization action of Ti-containing mixed molten slag were calculated by the equilibrium module of software Factsage with FToxid and FactPS databases (version 7.1). The chemical compositions of Ti-containing mixed molten slag, the addition mass of SiO_2, and CO_2

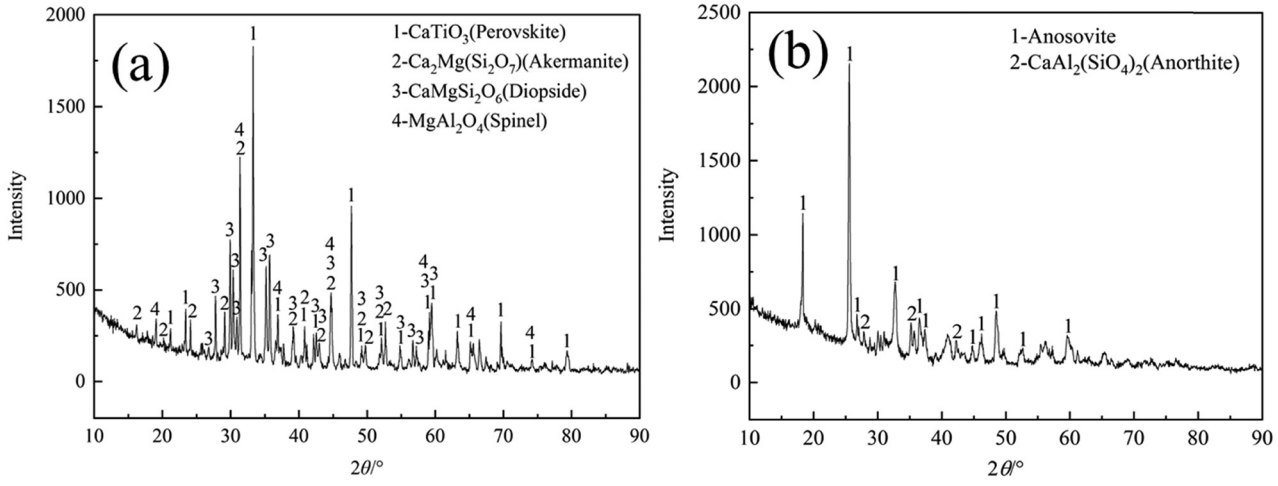

Figure 1: Phase compositions of (a) Ti-containing blast furnace slag and (b) Ti slag.

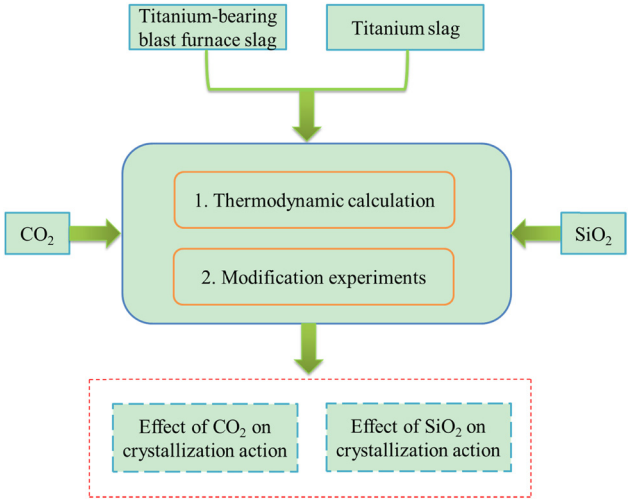

Figure 2: Schematic diagram of experimental process.

oxidation time were input into the software. Then, it will output the type and mass of precipitation phases.

2.2.2 Modification experiments

Based on the above-mentioned thermodynamic calculation, 278 g of Ti slag, 222 g of Ti-containing blast furnace slag, and a definite mass of silicon dioxide (50, 70, 90, and 110 g) were placed in a crucible at 1,460°C for 30 min. Whereupon, CO_2 was introduced into the mixed molten slag with a given time (60, 120, 180, and 240 s) and a flow rate of 4 L·min^{-1}. Afterward, the modification slag was cooled to room temperature with a cooling rate of 6°C·min^{-1}. The SiO_2 was of analytical grade, and the purity of CO_2 was 99% (mass fraction). The schematic diagram of the modified experimental device is shown in Figure 3. As shown in Figure 3, the heating equipment was a vertical $MoSi_2$ furnace with a B-type thermocouple. It was estimated that the overall absolute temperature accuracy of the furnace was ±3°C.

2.3 Characterization

The phase components were determined by X-ray diffraction (X'PERT PROMPD/PW3040). The microstructure and element distribution were determined by scanning electron microscopy (TESCAN VEGA III) equipped with an energy-dispersive spectrometer (INCA Energy 350).

3 Results and discussion

3.1 Thermodynamic calculation on CO_2 oxidation time

The addition mass of silicon dioxide was fixed at 50 g. After that, the influence of CO_2 oxidation time on the crystallization action of the mixed molten slag was investigated by software. The calculation results are illustrated in Figures 4–6.

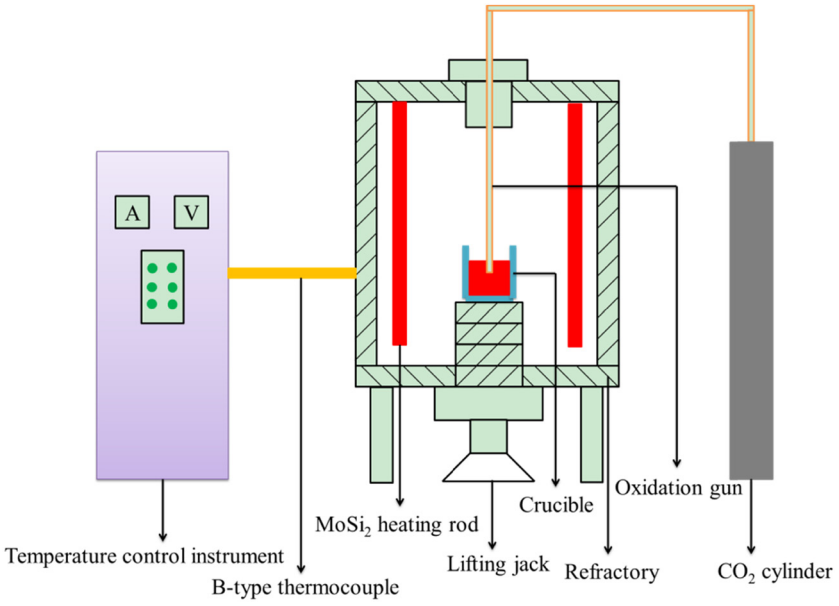

Figure 3: Schematic diagram of modified experimental device.

As illustrated in Figure 4a and b, the main titanium-bearing mineral phases are anosovite ($(AO{\cdot}2TiO_2)_m{\cdot}(B_2O_3{\cdot}TiO_2)_n$) and sphene ($CaSiTiO_5$) while the CO_2 oxidation times are 0 and 60 s. As illustrated in Figure 4c–f, the titanium-bearing mineral phases are rutile, sphene, and anosovite, while the CO_2 oxidation times are 120, 180, 240, and 300 s. It can be seen that other phases begin to precipitate when the mass of rutile precipitation reaches the maximum value. Moreover, as

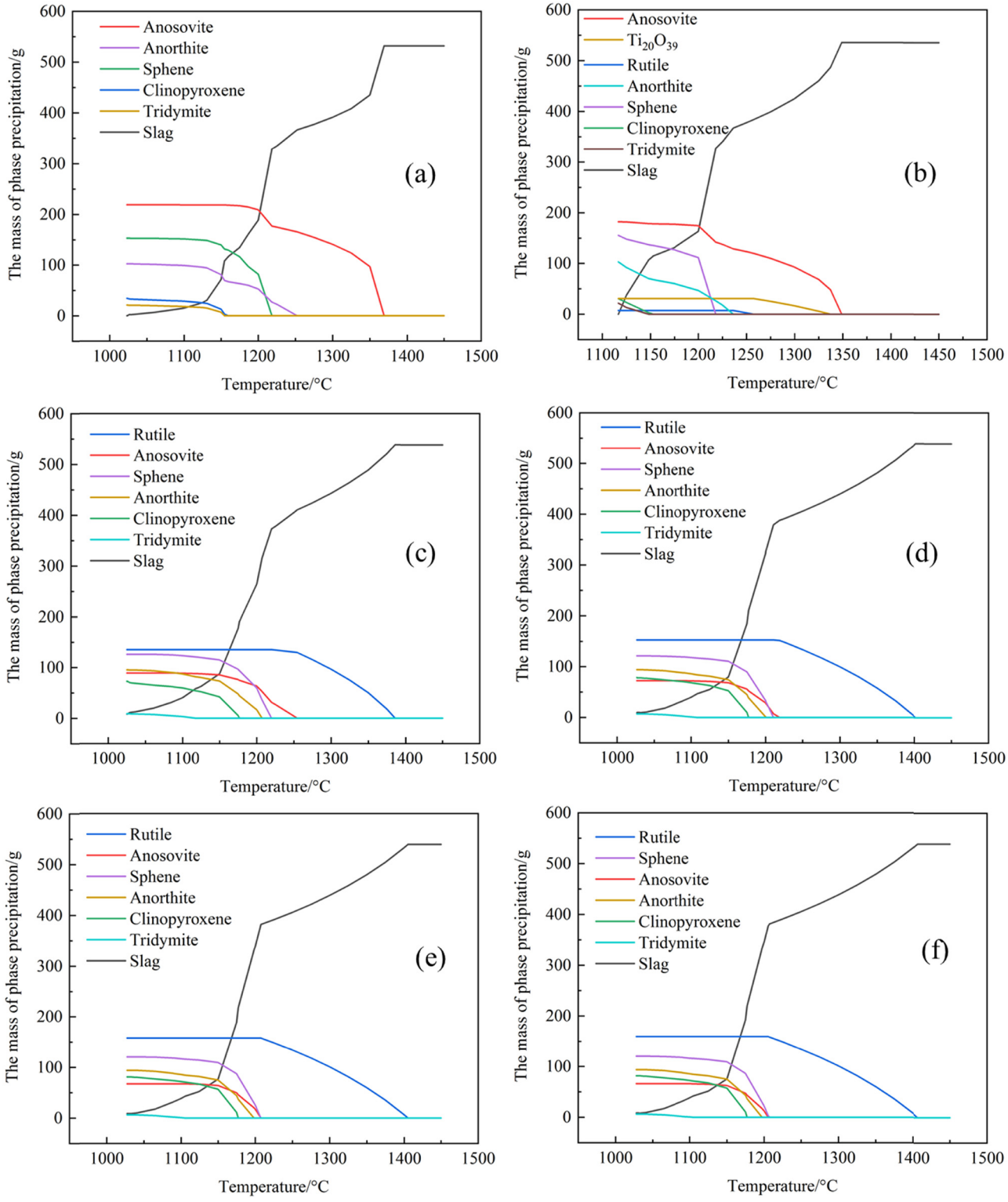

Figure 4: Effects of CO_2 oxidation time on the crystallization action: (a) 0 s, (b) 60 s, (c) 120 s, (d) 180 s, (e) 240 s, and (f) 300 s.

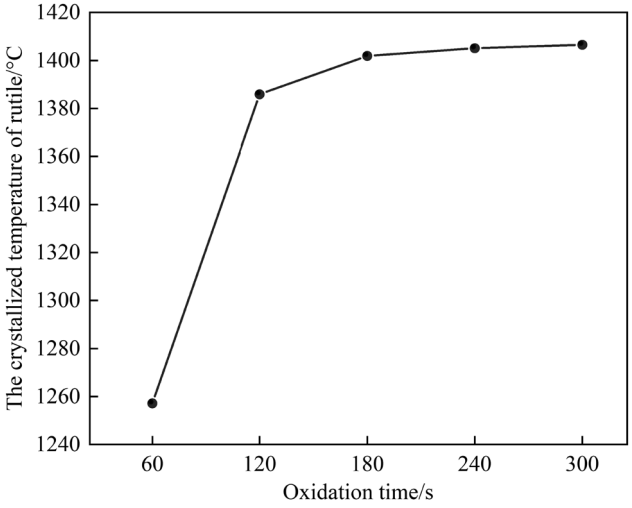

Figure 5: Effect of CO_2 oxidation time on the crystallized temperature of rutile.

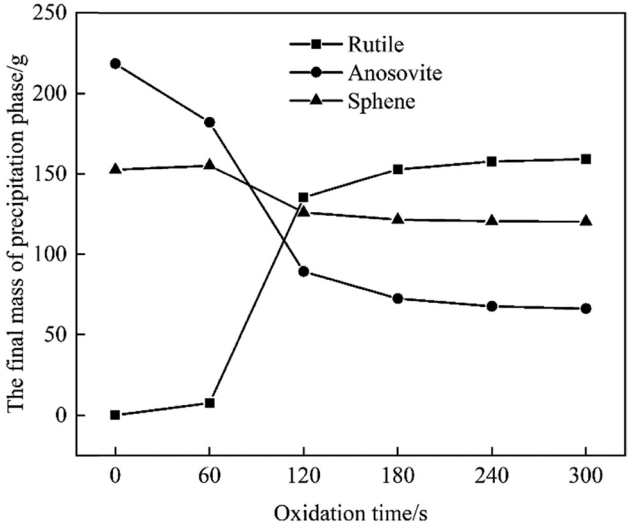

Figure 6: Influence of CO_2 oxidation time on the final mass of Ti-containing precipitation phases.

shown in Figure 5, the crystallized temperature of rutile rises as CO_2 oxidation time improves. To sum up, the improvement of CO_2 oxidation time can promote the crystallization of rutile crystals and inhibit the crystallization of other crystals.

As illustrated in Figure 6, with the CO_2 oxidation time improving from 0 to 180 s, the mass of rutile precipitation markedly rises, and the mass of anosovite and sphene precipitation decreases rapidly. As the CO_2 oxidation time improves to 300 s, the mass of rutile precipitation no longer improves, and the mass of anosovite and sphene precipitation no longer decreases. Therefore, the optimal CO_2 oxidation time is 180 s. It

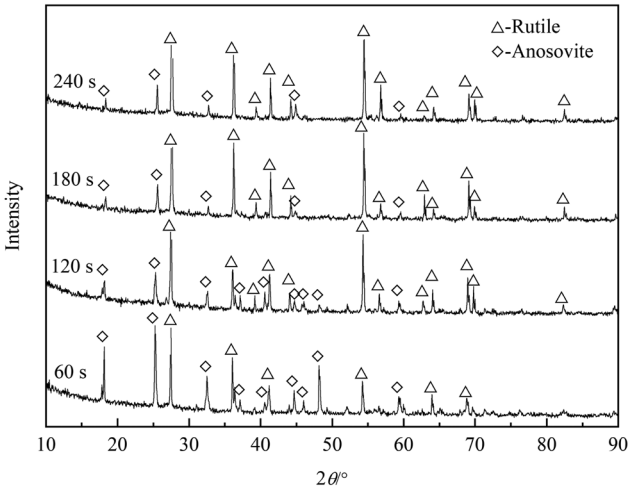

Figure 7: Phase components of the modification slags with diverse CO_2 oxidation times.

can be seen that the improving of CO_2 oxidation time can promote the transformation of anosovite and sphene to rutile.

3.2 Experimental verification on CO_2 oxidation time

The addition mass of silicon dioxide was fixed at 50 g. After that, the influence of CO_2 oxidation time on the crystallization action of the mixed molten slag was investigated by specific experiments. The experiment results are shown in Figures 7 and 8 and Table 2.

As illustrated in Figure 7, the phase components of the modification slag were unchanged while the CO_2 oxidation time was 60–240 s, that is, rutile and anosovite. Nevertheless, the diffraction peaks of anosovite reduced and the peak intensity significantly decreased when the CO_2 oxidation time increased from 60 to 180 s, meaning that the improvement of CO_2 oxidation time promoted the transformation of anosovite to rutile. It can be seen from Figure 8 and Table 2 that P3, P6, P9, and P12 were rutile. P2, P5, P8, and P11 were anosovite. P1, P4, P7, and P10 were matrix phases. The above-mentioned results imply that the phase components of the modification slag were rutile and anosovite while the CO_2 oxidation time was 60–240 s. Moreover, as the CO_2 oxidation time improved from 60 to 240 s, the Ti content of rutile reduced from 66.13 to 60.87 wt%, and the O content of rutile increased from 33.87 to 39.13 wt%. When the CO_2 oxidation time was 240 s, the mass ratio of Ti with O was 60.87/39.13. The ratio was close to the Ti/O mass ratio (6/4) of TiO_2, meaning that the improvement of CO_2 oxidation time

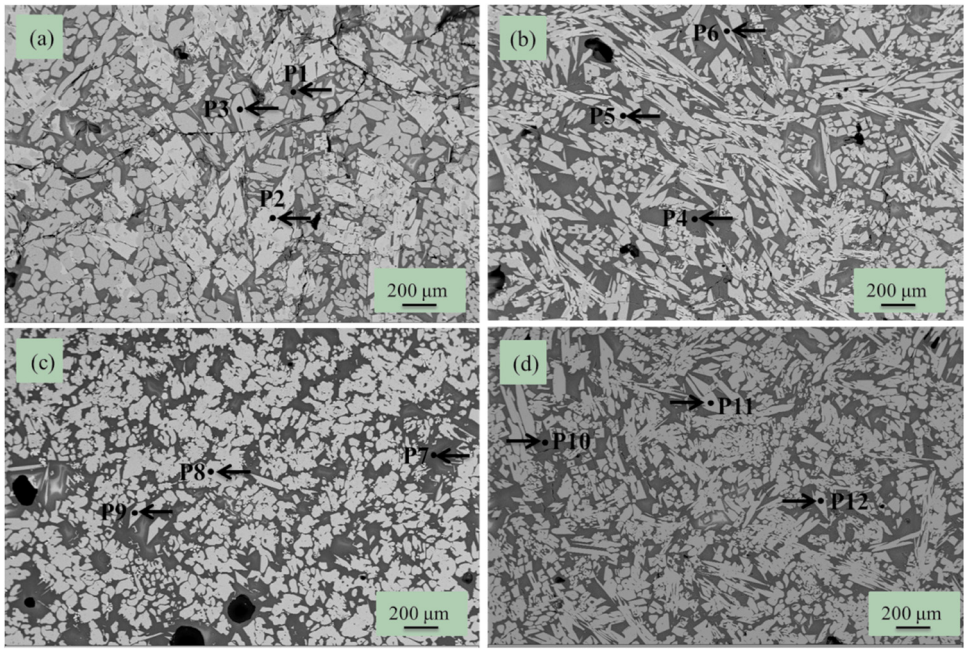

Figure 8: Microstructure of the modification slag with diverse CO_2 oxidation times: (a) 60 s, (b) 120 s, (c) 180 s, and (d) 240 s.

accelerated the transformation of anosovite to rutile. To sum up, the experimental results were consistent with the thermodynamic calculation results; that is, the improvement of CO_2 oxidation time accelerated the transformation of anosovite to rutile.

3.3 Thermodynamic calculation on the addition mass of SiO_2

The CO_2 oxidation time was fixed at 180 s. After that, the influence of the addition mass of silicon dioxide on the crystallization action of the mixed molten slag was investigated by FactSage software. The calculation results are shown in Figures 9–11.

As illustrated in Figure 9a–f, the Ti-bearing mineral phases are rutile, sphene, and anosovite while the addition mass of silicon dioxide is 30–130 g. Moreover, it can be seen that other phases begin to precipitate when the mass of rutile precipitation reaches the maximum value. As illustrated in Figure 10, the crystallization temperature of rutile raises as the addition mass of silicon dioxide improves. To sum up, the improvement of the SiO_2 addition mass can promote the crystallization of rutile crystals and inhibit the crystallization of other crystals.

Table 2: Element distribution of every point in Figure 8

Points	O (wt%)	Mg (wt%)	Al (wt%)	Si (wt%)	Ca (wt%)	Ti (wt%)	Mn (wt%)	Fe (wt%)
P1	36.85	8.74	14.03	16.79	14.11	2.73	3.41	3.34
P2	36.51	2.42	2.13			57.86	0.74	0.34
P3	33.87					66.13		
P4	37.42	8.36	13.15	16.82	14.64	2.03	3.69	3.89
P5	38.54	1.65	1.83			57.23	0.45	0.30
P6	36.48					63.52		
P7	37.51	8.17	13.74	16.55	14.43	2.19	3.74	3.67
P8	38.62	1.54	1.76			57.04	0.57	0.47
P9	38.53					61.47		
P10	37.41	8.03	14.12	16.27	14.75	2.04	3.89	3.49
P11	38.96	1.13	1.52			57.31	0.42	0.66
P12	39.13					60.87		

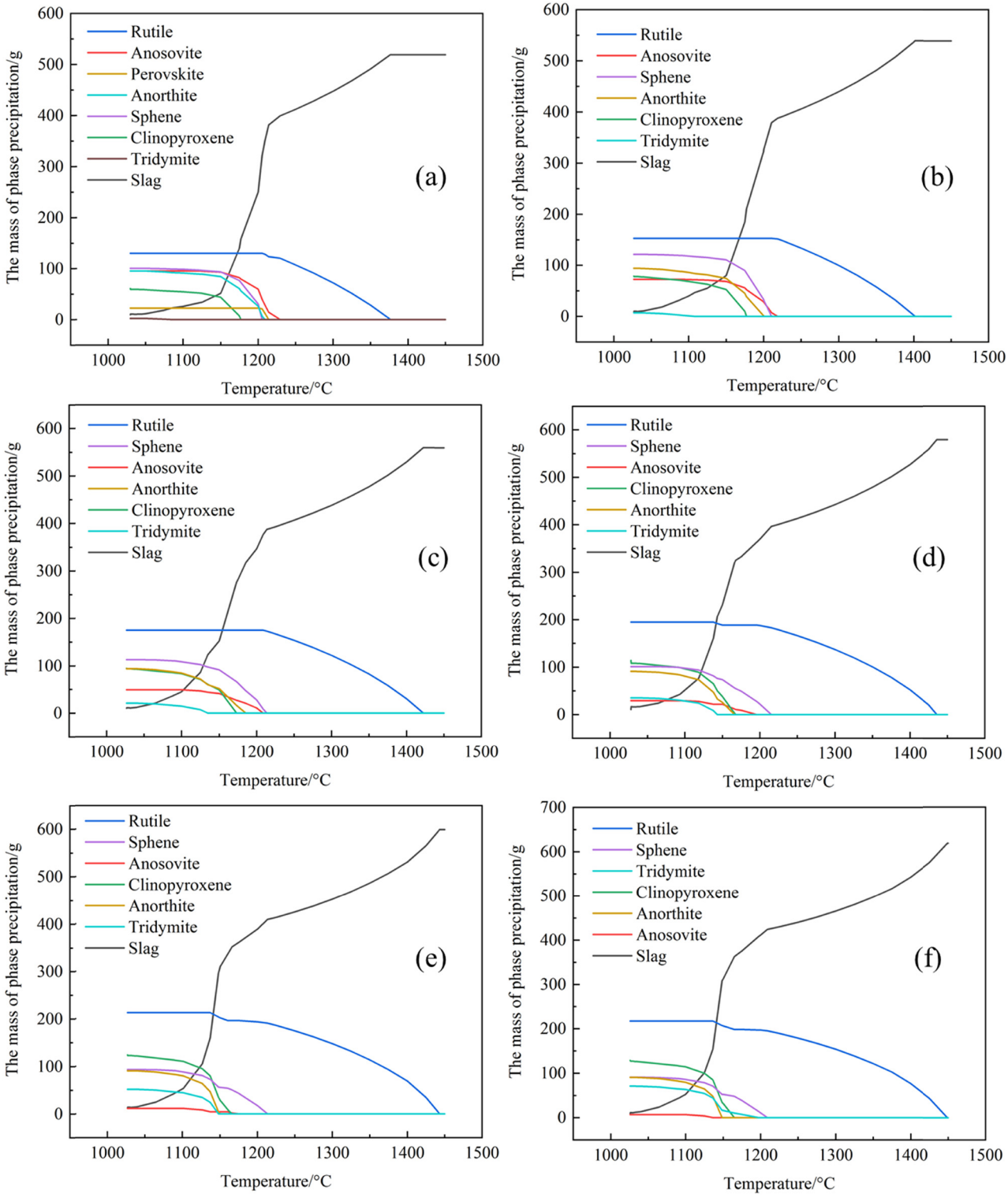

Figure 9: Effects of the addition mass of SiO_2 on the crystallization behavior: (a) 30 g, (b) 50 g, (c) 70 g, (d) 90 g, (e) 110 g, and (f) 130 g.

As illustrated in Figure 11, when the addition mass of silicon dioxide improves from 30 to 110 g, the mass of rutile precipitation observably improves, and the mass of anosovite and sphene precipitation decreases rapidly. With the addition mass of silicon dioxide improving to 130 g, the mass of rutile precipitation remained unchanged, and the mass of anosovite

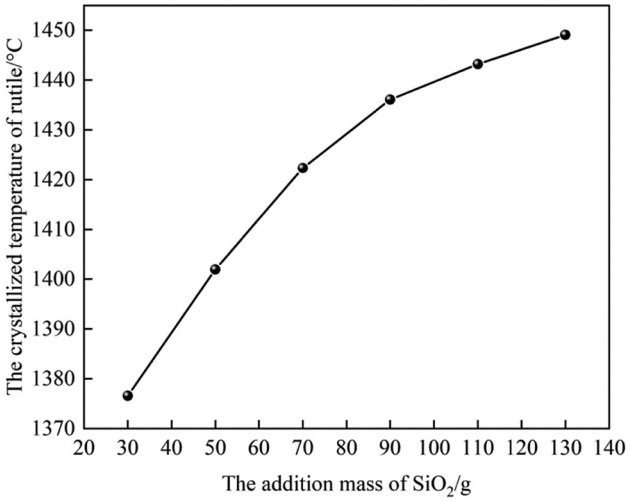

Figure 10: Effects of the addition mass of SiO_2 on the crystallized temperature of rutile.

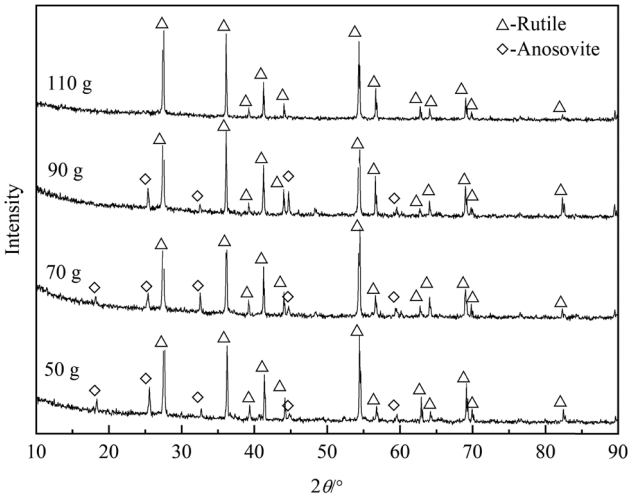

Figure 12: Phase components of the modification slags with diverse addition mass of SiO_2.

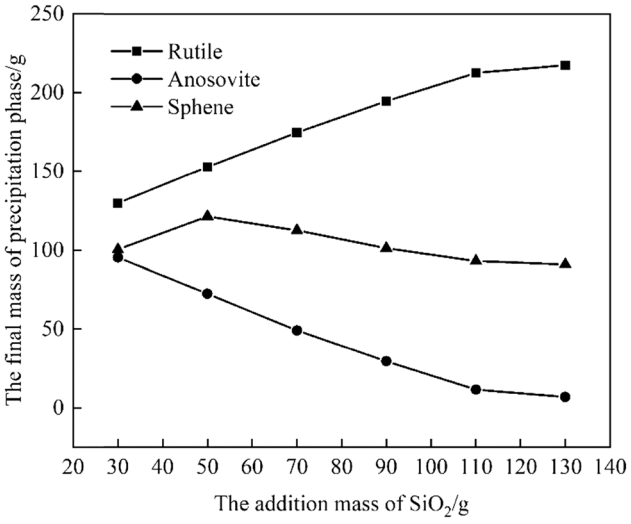

Figure 11: Effects of the addition mass of SiO_2 on the final mass of Ti-bearing precipitation phases.

and sphene precipitation also remained unchanged. Thus, the optimum addition mass of SiO_2 is 110 g. It can be seen that the improvement of the SiO_2 addition mass can promote the transformation of anosovite and sphene to rutile.

3.4 Experimental verification on the addition mass of SiO_2

The CO_2 oxidation time was fixed at 180 s. After that, the influence of the addition mass of silicon dioxide on the crystallization action of the mixed molten slag was investigated by relevant experiments. The experiment results are shown in Figures 12 and 13 and Table 3.

As illustrated in Figure 12, the phase component of the modification slag was unchanged when the addition mass of silicon dioxide improved from 50 to 90 g, i.e., rutile and anosovite. However, the diffraction peaks of anosovite reduced and the peak intensity significantly decreased. With the addition mass of SiO_2 improving from 90 to 110 g, anosovite phase disappeared, and the Ti-bearing phase of the modification slag was only rutile. Furthermore, it can be seen from Figure 13 and Table 3 that P2, P5, and P8 were all anosovite. P3, P6, and P9 were all rutile. P1, P4, and P7 were matrix phases. The above results imply that the phase components of the modification slag were rutile and anosovite when the addition mass of silicon dioxide was 50–90 g. With the addition mass of silicon dioxide improving from 90 to 110 g, the anosovite phase disappeared, and the Ti-bearing phase of the modification slag was only rutile. To sum up, the experimental results are consistent with the thermodynamic calculation results; that is, the improvement of the SiO_2 addition mass promoted the transformation of anosovite to rutile.

It can be seen from the above results that the thermodynamic calculation contained different phases, but the experiment did not. This is because theoretical calculation only considered thermodynamic conditions and ignored kinetic conditions. Because the purpose of this article was to obtain rutile, we only focused on the transformation of titanium-containing phases. According to the results of thermodynamic calculation, the main Ti-bearing phases (due to the very low mass of $Ti_{20}O_{39}$ and perovskite, they were ignored) were rutile, anosovite, and sphene. According

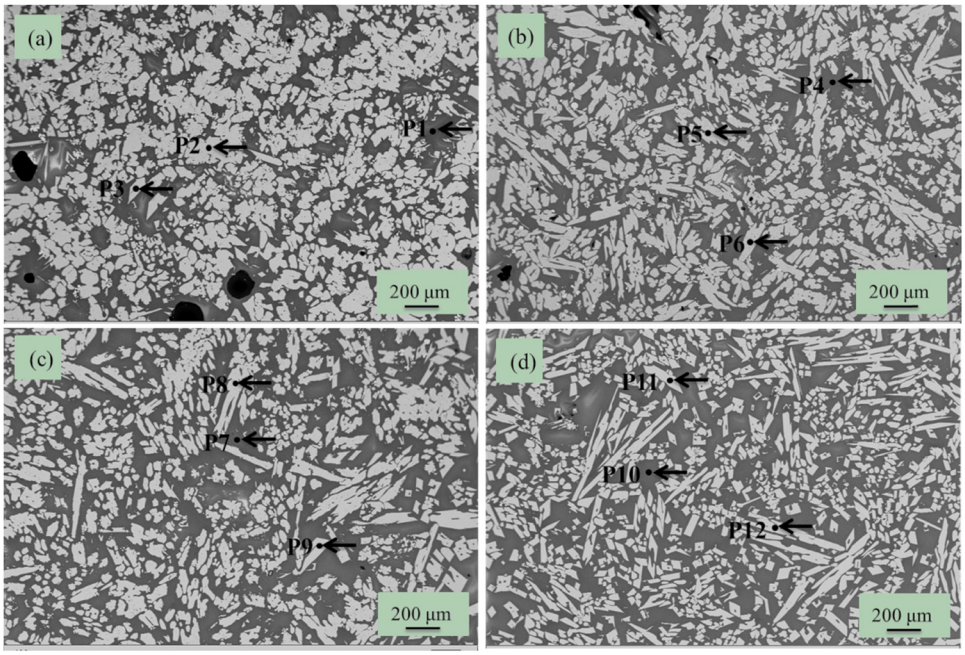

Figure 13: Microstructure of the modification slag with diverse addition mass of SiO_2: (a) 50 g, (b) 70 g, (c) 90 g, and (d) 110 g.

Table 3: Element distribution of every point in Figure 13

Points	O (wt%)	Mg (wt%)	Al (wt%)	Si (wt%)	Ca (wt%)	Ti (wt%)	Mn (wt%)	Fe (wt%)
P1	41.68	6.12	11.61	16.42	15.13	1.87	3.43	3.74
P2	42.36	7.56	6.89			39.57	1.13	2.49
P3	35.45					64.55		
P4	38.42	7.53	12.13	16.89	15.02	2.16	3.56	4.29
P5	41.13	6.03	5.13			45.26	0.86	1.59
P6	35.87					64.13		
P7	36.75	8.65	13.42	17.13	13.46	2.36	3.42	4.81
P8	40.76	3.37	2.34			52.26	0.51	0.76
P9	36.47					63.53		
P10	36.02	10.15	13.78	17.47	13.14	1.43	3.87	4.14
P11	40.45					59.55		
P12	40.51					59.49		

to the results of experiments, the main Ti-bearing phases were rutile and anosovite. It can be seen that the theoretical calculation results were consistent with the experimental results. The only difference is that the titanium-bearing phases of the experimental results did not include sphene. This may be because thermodynamic calculation ignored the effect of kinetics conditions.

3.5 Theory of rutile precipitation

In order to investigate the theory of rutile precipitation, the standard Gibbs free-energy changes (ΔG^{Φ}) of relevant reactions were calculated by the reaction module of Factsage software. The calculation results are illustrated in Figure 14.

As illustrated in Figure 14, the products of reactions (4–7) are all anosovite. The ΔG^{Φ} of reactions (1) and (2) are less than those of reactions (3–5), meaning that reactions (3–5) are restrained as the addition mass of SiO_2 improves. In other words, the precipitation of anosovite and perovskite is inhibited. Thus, the addition of SiO_2 can promote the conversion of anosovite and perovskite to Ti oxides (TiO_2, Ti_3O_5, Ti_2O_3, and TiO). As shown in Figure 14, the ΔG^{Φ} of reactions (8–12) is less than those of reactions (6–7), indicating that reactions (6–7) are restrained as CO_2 oxidation

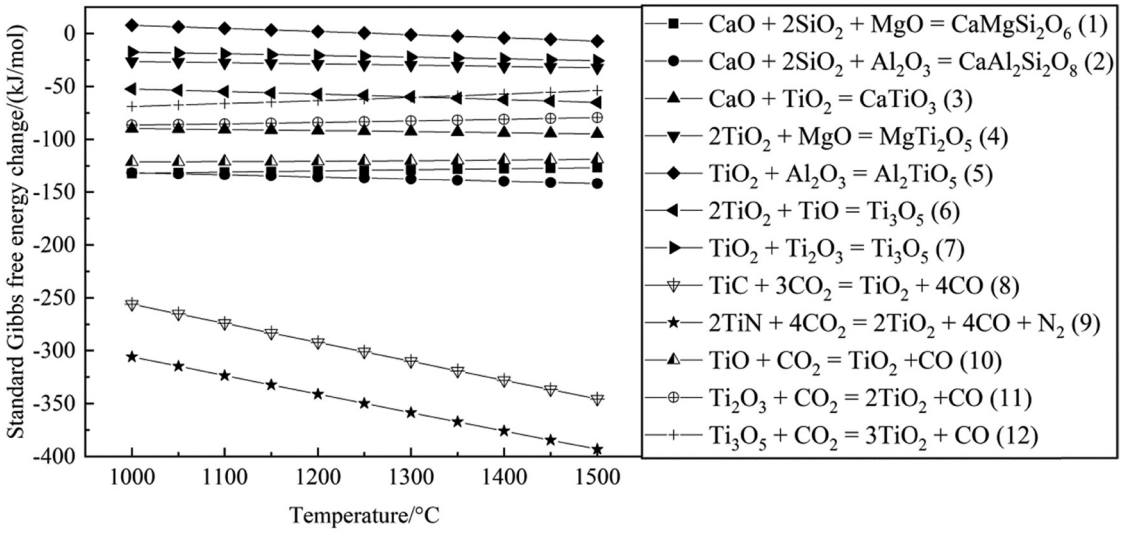

Figure 14: ΔG^{Φ} of reactions 1–12.

time improves. In other words, the precipitation of anosovite is inhibited. It is well known that anosovite is a solid solution based on Ti_3O_5. Thus, CO_2 oxidation can eliminate low-valent titanium oxides including Ti_3O_5 and promote the transformation of anosovite into rutile. To sum up, reactions (3–7) are restrained, and Ti compositions are present as rutile while CO_2 and SiO_2 are concurrently added to the mixed molten slag.

4 Conclusions

1. The improvement of SiO_2 addition mass and CO_2 oxidation time can promote the transformation of anosovite to rutile.
2. The optimal experiment conditions were the SiO_2 addition mass of 110 g and the CO_2 oxidation time of 180 s, and the phase composition of slag was only rutile under the above conditions.
3. Using CO_2 as an oxidizing gas can not only prepare rutile but also achieve carbon neutrality, which is a clean preparation method.

Funding information: This work was supported by Funding Project for National Science and Technology Support Program of China (grant number: 2015BAB18B00).

Author contributions: Li Zhang: methodology, resources; Jiqing Han: writing – original draft, writing – review and editing, visualization, methodology; Qiuping Feng: writing – review and editing.

Conflict of interest: The authors state no conflict of interest.

Data Availability Statement: The datasets generated during and/or analysed during the current study are available from the corresponding author on reasonable request.

References

[1] Yang H, Zhao S. Comprehensive utilization of BF slags in building materials. Conserv Util Miner Resour. 2004;1:47–51.
[2] Zhou XL, Lu XG. Preparation of titanium alloy by direct reduction of Ti-bearing blast furnace slag. Chin J Nonferrous Met. 2010;20(9):1829–35.
[3] Lei XF, Xue XX. Effect of sulfate on photocatalytic activity of titanium-bearing blast furnace slag. Mater Rep. 2009;23(2):63–6.
[4] Yan F, Li C, Liang B. A two-step sulfuric acid leaching process of Ti-bearing blast furnace slag. Chin J Process Eng. 2006;3:413–7.
[5] Gao YM, Li CY, Li YW. Analysis of carbothermal reduction of TiO_2 and extraction of titanium carbonitride from the blast furnace slag bearing titania. J Wuhan Univ Sci Technol. 2007;30(1):5–9.
[6] Li YH, Lou TP, Sui ZT. Selective enrichment of Ti component in Ti-bearing blast furnace slag and precipitation behavior of perovskite phase. Chin J Nonferrous Met. 2000;5:719–22.
[7] Li J, Zhang ZT, Zhang M, Guo M, Wang XD. The influence of SiO_2 on the extraction of Ti element from Ti-bearing blast furnace slag. Steel Res Int. 2011;82(6):607–14. doi: 10.1002/srin.201000217.
[8] Ren S, Zhao Q, Yao L, Liu QC. Precipitation behavior of perovskite and anosovite crystals from high Ti-bearing blast furnace slag with small amount of B_2O_3. CrystEngComm. 2016;18(8):1393–402. doi: 10.1039/c5ce02131f.
[9] Zhang L, Zhang JH, Zhang W, Li GQ. Thermodynamic analysis of extraction of synthetic rutile from modified slag. Ind Eng Chem Res. 2013;52(13):4924–31. doi: 10.1021/ie301414h.

[10] Zhang W, Zhang L, Zhang JH, Feng NX. Crystallization and coarsening kinetics of rutile phase in modified Ti-bearing blast furnace slag. Ind Eng Chem Res. 2012;51(38):12294–8. doi: 10.1021/ie3007825.
[11] Zhang W, Zhang L, Li YH, Li X. An environmental procedure to extract titanium components and metallic iron from Ti-bearing blast furnace slag. Green Process Synth. 2015;4(4):307–16. doi: 10.1515/gps-2015-0031.
[12] Zhang W, Zhang L, Li YH, Li X. Crystallization behavior and growing process of rutile crystals in Ti-bearing blast furnace slag. High Temp Mater Processes-Isr. 2016;35(8):787–97. doi: 10.1515/htmp-2015-0103.
[13] Li J, Wang XD, Zhang ZT. Crystallization behavior of rutile in the synthesized Ti-bearing blast furnace slag using single hot thermocouple technique. ISIJ Int. 2011;51(9):1396–402. doi: 10.2355/isijinternational.51.1396.
[14] Sun YQ, Li J, Wang XD, Zhang ZT. The effect of P_2O_5 on the crystallization behaviors of Ti-bearing blast furnace slags using single hot thermocouple technique. Metall Mater Trans B. 2014;45(4):1446–55. doi: 10.1007/s11663-014-0077-0.
[15] Du Y, Gao JT, Lan X, Guo ZC. Selective precipitation and in situ separation of rutile crystals from titanium bearing slag melt in a super-gravity field. CrystEngComm. 2018;20(27):3868–76. doi: 10.1039/C8CE00678D.
[16] Du Y, Gao JT, Lan X, Guo ZC. Recovery of rutile from Ti-bearing blast furnace slag through phase transformation and super-gravity separation for dielectric material. Ceram Int. 2020;46(7):9885–93. doi: 10.1016/j.ceramint.2019.12.264.
[17] Zhang JH, Han JQ, Chen X, Zhang J, Zhang L. Experimental study on titanium-containing mixed slag. Light Met. 2021;09:40–4.
[18] Han JQ, Zhang J, Zhang JH, Chen X, Zhang L, Tu GF. Recovery of Fe, V and Ti in modified Ti-bearing blast furnace slag. Trans Nonferrous Met Soc China. 2022;32(1):333–44. doi: 10.1016/S1003-6326(22)65798.
[19] Han JQ, Zhang J, Zhang JH, Chen X, Zhang L, Tu GF. Extraction of vanadium and enrichment of titanium from modified Ti-bearing blast furnace slag. Hydrometallurgy. 2021;201(1):1–10. doi: 10.1016/j.hydromet.2021.105577.
[20] Han JQ, Zhang JH, Chen X, Zhang J, Zhang L, Tu GF. Effect of rutile crystal shapes on its settlement. Trans Nonferrous Met Soc China. 2020;30(10):2848–60. doi: 10.1016/S1003-6326(20)65426-7.